Characterizing Topological Insulators for High-Performance Electronics (Computational Analysis)

Ethan Raisbeck

March 7, 2021

Abstract

Topological Insulators (TI) are a relatively new class of material with interesting charge transport properties. The recently discovered time reversal invariant TI's classified by the $\mathbb{Z}2$ invariants will be the subject of this report. Relativistic effects allow the appearance of Topological surface states with the ability to transport Dirac fermions with very little resistance. In this report, Topological Insulators Bismuth (III) Selenide and Antimony (III) Telluride are examined to evaluate how they will be beneficial for High-Performance devices. Computational analysis is used to investigate different effects from magnetoresistance and Hall resistance data, such as Shubnikov–de Haas oscillations and the dependence of carrier mobility on temperature. It is also attempted to observe the samples showing exotic properties such as a 2D Dirac surface state and linear magnetoresistance, which would be beneficial to a high-performance device. Linear magnetoresistance was observed, although it will be concluded that that the observed quantum oscillations do not indicate a 2D Dirac surface state. Additionally it will be concluded that there is an exponential decrease in charge mobility with an increase in temperature.

Contents

Chapter 1

Introduction

1.1 Topology

Topology is a mathematical concept whereby an object can be deformed in any way that does not include it being teared or attached to itself. A common example of this is using a doughnut and a teacup. These two objects are said to be topologically identical, meaning they are within the same topological class, as they can be moulded into each other without any tearing or sticking together. A solid spherical object without a hole in it such as an apple would be in a different topological class.

This follows that different classes of shapes can be classed by a topological invariant, which corresponds to the number of holes they contain. In condensed matter physics, the topological invariant is also classed by other effects such as time-reversal symmetry and particle-hole symmetry [1]. For TI's of the same topological invariant, the Hamiltonian operator can be freely changed to alter the band structure of the material; Providing that the Fermi level does not fall within any available quantum states, the properties of the material will be conserved.

1.2 Band structure

Topological Insulators have a small band gap, hence they used to be called narrow band-gap semiconductors [2][3]. This means that it takes a small amount of energy to excite electrons between the valence and conduction bands. Usually for an semiconductor, this would mean that it can only conduct electricity in certain conditions because the electrons won't always have the energy to move to the conduction band, where there are free quantum states which an electron can move through. However, topological insulators have the ability to be able to swap quantum states between valence and conduction bands due to large spin orbit interactions relative to other materials. This allows for an edge state, which is a conducting layer around the bulk of the material.

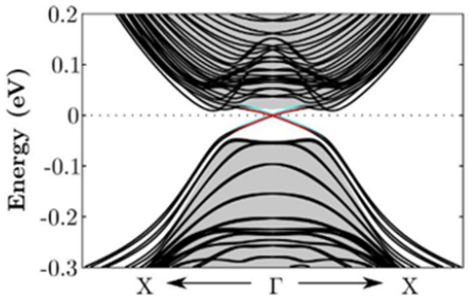

Figure 1.1: An example band structure of TI Bi_2Se_3 showing a small band gap joined by the surface states shown in red [4].

1.3 Quantum spin Hall effect

A useful analogy for understanding charge transport within a 2D TI would be to compare it to the quantum spin Hall effect, as the Topological surface state shows properties similar to this state [5]. When a material is placed within a perpendicular magnetic field, the Lorentz force will act on the charge carriers in the direction perpendicular to the current flow and magnetic field. In a sufficiently high magnetic field, the Lorentz force is so strong that carriers move in cyclotron orbits, where the cyclotron frequencies are quantised into Landau levels. At the edge of the material (in the 'edge' state), the orbits are unable to complete, hence the carriers are able to break out of the cyclotron motion and contribute towards charge transport within this edge state. For TI's this happens naturally (without the magnetic field) because of the strong spin-orbit interactions creating an internal magnetic field.

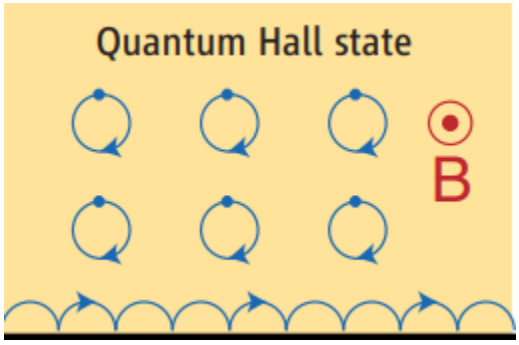

Figure 1.2: An image to show the movement of electrons in a quantum Hall state which is analogous to charge transport within a 2D TI. In the bulk of the material the electrons move in quantised cyclotron orbits where they are unable to transfer current. The conducting edge states enable electrons to move freely along the surface of the material [6].

1.4 Shubnikov–de Haas oscillations (SdH)

The quantisation of the density of states into Landau levels within materials such as TI's are the reason for certain phenomena such as quantum (SdH) oscillations at high magnetic fields [7]. As the magnetic flux density is increased, clear gaps begin to form inbetween the Landau levels. When the Fermi level falls within the gaps, there are no available quantum states unless the charge carrier is able to scatter between the highest full Landau level to the empty one above. This is possible, but in order to minimise this and observe clear Landau quantisation, the system is kept at low temperature (just above 0K) where the Fermi energy is far greater than the cyclotron frequency, so that only inelastic scattering events can take place [8]. Since no elastic scattering events are possible, the resistivity of the surface state at this point is very small. When the Fermi level falls within a Landau level, a spike in resistivity can be observed since there are free quantum states within the same Landau level, allowing elastic scattering.

1.5 Mobility of charge carriers

Mobilities are important values to be obtained from TI's with regards to their performance in a high-performance device. For a device to work efficiently and have low response time, a high mobility is essential [9]. In a transistor, if a charge carrier has a high mobility then it also has a higher drift velocity which can charge capacitors more rapidly, leading to a faster device response. As transistors form the basis for all high-performance devices, carrier mobility is a very important property [9].

1.6 Spin-Orbit Interactions

Spin-Orbit Interactions are an important relativistic effect which allows for the non-trivial topologically protected surface states (also called edge states or boundary states). Spin-orbit interactions allow for the phenomena whereby the density of states in the valence band can be partially swapped with that in the conduction band. When changing topological invariance, a surface state in the forbidden energy gap of the band structure is formed which is between the non-trivial (topological) state and the trivial state. This allows for the conduction of electrons on the 2D surface of a material at very low temperatures despite having a band gap with the magnitude of a conventional semiconductor.

Strong spin orbit interactions also mean that the spin and momentum of the electrons in the surface state are locked perpendicular to each other. Electrons under these conditions are named helical Dirac fermions [10], which are always in pairs of opposite spins, as stated by Kramers degeneracy theorem [11][12]. This allows for lanes of current that flow in a direction dictated by the spin quantum numbers of the fermions. It also means that two lanes of current can flow in opposite directions to each other whilst being unable to interact which is a useful property for electrical devices.

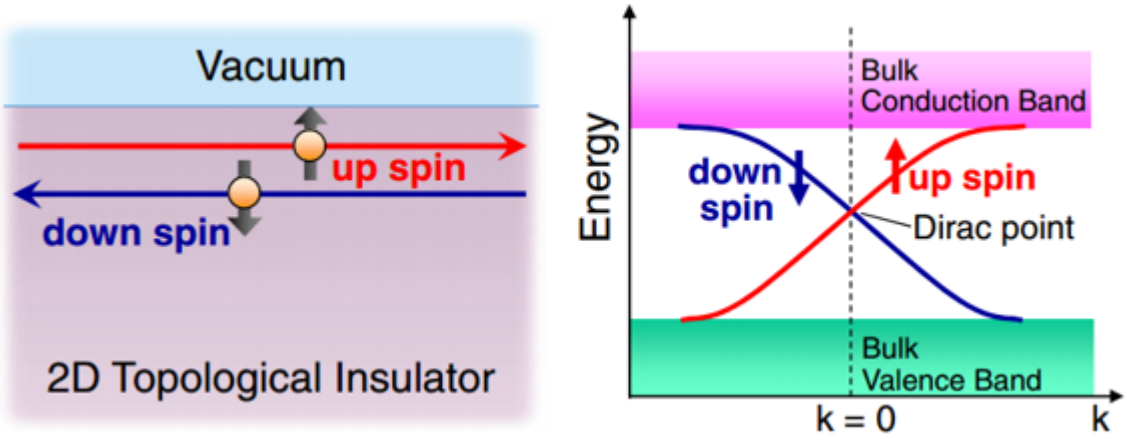

Figure 1.3: The left diagram shows how the helical Dirac fermions come in Kramers pairs with opposite spin which travel in opposite directions. The right diagram shows the surface state in the energy gap between conduction and valence bands as a result of spin-orbit interactions, converging at the Dirac point.[10]

A direct consequence of large spin-orbit interactions is the ability to prevent scattering of electrons, which suppresses electrical conductivity on typical conductive materials such as metals [9]. The topological protection also prevents other impurities and perturbations interfering with the charge transport channels within the surface state. A very low resistivity and high mobility of carriers results from this, making TI's very useful for high-performance devices. The lack of scattering events also means the transistors would experience less joule heating [9], which is a current problem in traditional semiconducting devices.

1.7 Dirac model

Charge carriers in TI's are described as relativistic Dirac fermions through the Dirac equation (equation 1.1) [11]. Some TIs' show a band structure close to the Fermi level named a Dirac cone (Figure 1.4). The valence and conduction bands of the linear dispersion relation shown by some TI's and related by time-reversal symmetry, cross at the time-reversal invariant momentum, also called the Dirac point [13]. The relativistic effect of Dirac fermions in the Dirac cone shaped dispersion relation corresponds to high Fermi velocities [14] which can give very high carrier mobilities.

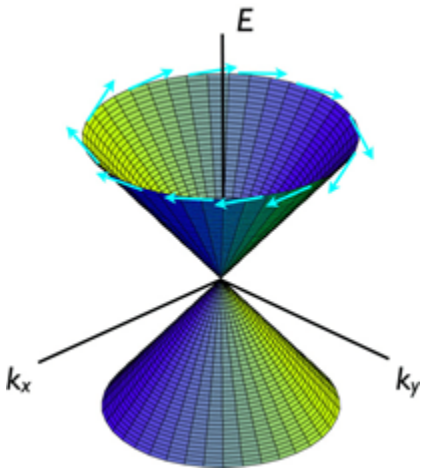

Figure 1.4: A visual representation of a 3D band structure from a TI showing a single Dirac cone as a function of energy and wavevector. The arrows indicate the helical spin polarization of Dirac fermions [10][15].

Dirac fermions are modelled as massless relativistic particles using the Dirac equation [16]. α_n and β are 4x4 Hermitian and involution matrices respectively, p_n are the components of momentum, $\psi(x,t)$ is the Schrödinger equation as a function of position x and time t and m is the rest mass for the fermion.

$$\left(\beta mc^2 + c\sum_{n=1}^{3}\alpha_n p_n\right)\psi(x,t) = i\hbar\frac{\partial\psi(x,t)}{\partial t} \tag{1.1}$$

1.8 Weak antilocalisation effect (WAL)

WAL is an effect which occurs at zero and low magnetic fields, caused by spin-momentum locking of fermions which decreases scattering events. This effect dominates the contribution to conductivity at low magnetic fields, which is an important property of TI's that would make them useful in high-performance devices.

Kramers degeneracy theorem [12] states that fermions in the Dirac surface state will travel in pairs of opposite spin around a closed loop (as in the wrapped state in Figure 1.2). The interaction between the spins of fermions travelling in opposite directions interfere destructively [17]. This causes a decrease in backscattering which in turn decreases the resistivity. The WAL effect is only seen at low field since the presence of an external field will break time-reversal symmetry, causing a loss of phase coherence[18], meaning there is no longer destructive interference for the WAL effect.

1.9 Berry phase

The Lifshitz Kosevich theory can be used to express quantum oscillations with the change in magneto-conductivity as

$$\Delta\sigma_{xx} = A_0 R_T R_D R_S cos[2\pi(\frac{F}{B} - \frac{1}{2} + \beta)] \tag{1.2}$$

Where the coefficients A_0, R_T, R_D, R_S and β are a dimensionless constant, the temperature, Dingle, and spin damping factors and the Berry phase respectively [10][19]. For this report, this equation

will be simplified for the purpose of ease of fitting the equation as

$$\Delta\sigma_{xx} = \alpha cos[2\pi(\frac{F}{B} - \frac{1}{2} + \beta)] \tag{1.3}$$

A Landau fan diagram can be plotted to extract the Berry phase which will determine the nature of the fermions in the surface state. This is possible as the minima/maxima of the quantum oscillations denoted by a Landau index number N will match the minima/maxima of the cosine function at $2(N-1)\pi$. The Landau fan diagram can then be created where the x-intercept will yield the Berry phase, using the relationship

$$\frac{F}{B} + \beta = N \tag{1.4}$$

A non-trivial Berry phase value of 0.5 or π will indicate the presence of Dirac fermions [10] in the surface state. Conversely, a value of 0 will indicate a non-topological surface state [20] without the presence of Dirac fermions.

Chapter 2

Methods

2.1 Growth of samples

Both samples of Bismuth (III) Selenide and Antimony (III) Telluride were synthesised using a modified Bridgman method. Layered units were exfoliated from bulk samples by breaking the Van der Waals bonds. There was a cooling rate of 6°C per hour from 705°C to 515°C with a temperature gradient of approximately 2°C/mm [21].

2.2 Experimental methods

To extract useful quantities of a topological insulator, the only variable measured is the voltage across the sample. The voltage is measured along and across the sample as longitudinal and transverse voltage. This is done by using 6 points of contact with the sample, two for the current and four for the voltages.

It is impossible for these contacts to have no effect on the electric field on the surface of the sample, which will effect current flow. This means that non uniform current distribution will occur as a result of this and to mitigate the effect as much as possible, the voltage points of contact are placed towards the middle of the sample. Due to this the inevitable non uniform current distribution, the data has to be symmetrised, as shown in section 2.3.

For each sample, an electromagnet with a magnetic field perpendicular to the flow of charge through the TI was set up. The longitudinal and transverse voltage was recorded whilst varying the electromagnet between -8T and +8T. The raw data also contained measurements for when the electromagnet was powering up and down which was removed in the analysis.

2.3 Analysis techniques

To begin analysis for the samples of TI's, the same base process was used each time. The aim is to obtain two graphs for each sample of the magnetoresistance and Hall Resistance data as any further analysis requires these. The process of plotting these graphs using Python from the raw voltage data is outlined as follows:

1) Import the in-phase transverse/longitudinal voltage and magnetic flux density data

2) Separate the useful Magnetic Flux Density and Voltage data from the whole data set to reduce noise as the data from when the electromagnet is powering up and down is not useful

3) Interpolate the data to create a continuous data set

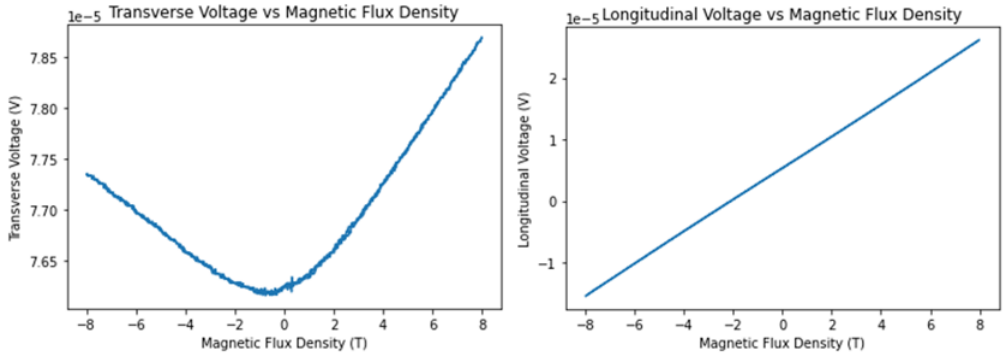

Figure 2.1: Raw imported longitudinal and transverse voltage data from Bi_2Se_3

4) Convert the resistance data to resistivity using sample dimensions

5) Symmetrise and asymmetrise the resistivity data using the following equations to account for non uniform current distribution

$$\rho_{xx}(B) = \frac{\rho^0_{xx}(B) + \rho^0_{xx}(-B)}{2} \tag{2.1}$$

$$\rho_{yx}(B) = \frac{\rho^0_{yx}(B) - \rho^0_{yx}(-B)}{2} \tag{2.2}$$

2.4 2-band model

If one were to assume that the band structure of the analysed TI's only contains two bands, the magnetoresistance (equation 2.3) and Hall resistance (equation 2.4) as a function of magnetic flux density can be described using the following equations, where μ and n are the mobility and carrier density for electrons (e) and holes (h)[22].

$$\rho_{xx}(B) = \frac{1}{e} \cdot \frac{(n_h\mu_h + n_e\mu_e) + (n_h\mu_e + n_e\mu_h)\mu_h\mu_e B^2}{(n_h\mu_h + n_e\mu_e)^2 + (n_h - n_e)^2\mu_h^2\mu_e^2 B^2} \tag{2.3}$$

$$\rho_{yx}(B) = \frac{B}{e} \cdot \frac{(n_h\mu_h^2 + n_e\mu_e^2) + (n_h + n_e)\mu_h^2\mu_e^2 B^2}{(n_h\mu_h + n_e\mu_e)^2 + (n_h - n_e)^2\mu_h^2\mu_e^2 B^2} \tag{2.4}$$

The two band model is used to extract the mobility and carrier density for holes and electrons by using them as fitting coefficients. In reality there are far more than two bands (as in Figure 1.1), however limiting the model to only show two will give adequate values whilst avoiding unnecessary complexity. This model is only used when contributions to the Hall resistivity can be seen from more than one band, which is when there is non-linear Hall data.

2.5 1-band model

The 1-band model is not usually a conventional model, however it is used when there is no clear resistivity contribution from 2-bands, hence negating the need for the more complex 2-band fitting. Linear Hall data shows that most of the mobility contribution is from one band. This means one can approximate that the mobility and carrier density for both bands is the same. A derivation of the 1-band model is

shown as follows, starting from the 2-band model in equation 2.3.

$$\rho_{xx}(B) = \frac{1}{e} \cdot \frac{(n_h\mu_h + n_e\mu_e) + (n_h\mu_e + n_e\mu_h)\mu_h\mu_e B^2}{(n_h\mu_h + n_e\mu_e)^2 + (n_h - n_e)^2\mu_h^2\mu_e^2 B^2} \tag{2.5}$$

At $B = 0$

$$\rho_{xx}(0) = \frac{1}{e} \cdot \frac{1}{(n_h\mu_h + n_e\mu_e)} \tag{2.6}$$

At low magnetic flux density one can approximate

$$\rho_{xx}(B) = \rho_{xx}(0)(1 + \mu_h\mu_e B^2) \tag{2.7}$$

Approximate that $\mu_h = \mu_e = \mu$

$$\rho_{xx}(B) = \rho_{xx}(0)(1 + \mu^2 B^2) \tag{2.8}$$

This is the equation to which the magnetoresistance data is fitted too at low magnetic flux density, allowing the extraction of the mobility.

Chapter 3

Results and Analysis

3.1 Antimony (III) Telluride

The sample of Sb_2Te_3 was used to evaluate the effect of temperature change on the mobility of the sample. The sample had excess Te in growth that would lead to a higher mobility than expected for perfect Sb_2Te_3 [21]. Data from the sample was taken at seven different low temperatures ranging from 0K to 30K. Magnetoresistance and Hall resistance graphs are shown for each temperature.

3.1.1 Hall data

The Hall data shows a positive gradient which gives a positive Hall coefficient of $(3.60\pm0.01)\times10^{-8}m^3C^{-1}$, indicating that this sample of Sb_2Te_3 is p-type, meaning that holes are the majority charge carrier. The value of the carrier density is also obtained through the Hall coefficient which is $(1.74\pm0.01)\times10^{20}cm^{-3}$. This is a fairly high carrier density for Sb_2Te_3 with regards to other samples from literature [23][24].

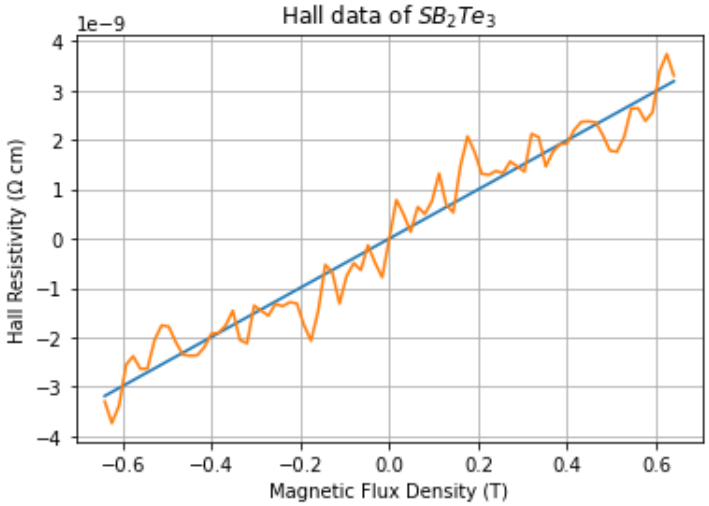

Figure 3.1: Hall data from the sample of Sb_2Te_3 at low field, showing the positive gradient and the fitting used to extract the Hall coefficient.

3.1.2 Magnetoresistance data

The mobilities for each temperature were obtained through using the 1-band model on the magnetoresistance data, which proved to be very inaccurate, most likely because the data contains a lot of noise. This

was also one of the reasons for not using the 2-band model for this sample, even though 2-band contribution can be seen in the Hall data. The mobility values obtained vary from approximately $2300cm^2V^{-1}s^{-1}$ to $3600cm^2V^{-1}s^{-1}$ with a sharp increase up the $3600cm^2V^{-1}s^{-1}$ for the 30K data, which vaguely aligns with the percentage change in mobility graph in section 3.1.4. The mobility values obtained through this fitting, as well as the attempted fitting are far higher than would be expected. One may observe (Figure 3.4) that there are no SdH oscillations in this data which would be expected to start at a relatively low magnetic flux density with mobility values this high. The high value could be caused by the excess Te from the growth of the sample and the high amount of noise in the data resulting in inaccurate fittings.

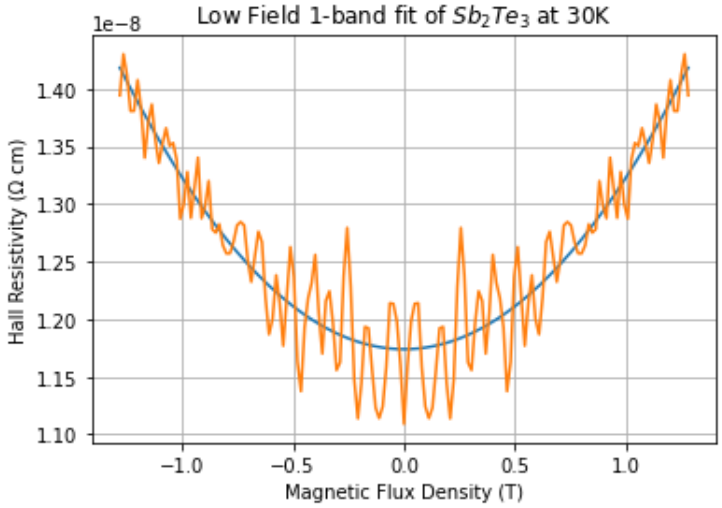

Figure 3.2: 1-band fitting of Sb_2Te_3 at 30K, showing a large amount of noise leading to large uncertainties

3.1.3 Temperature dependence data

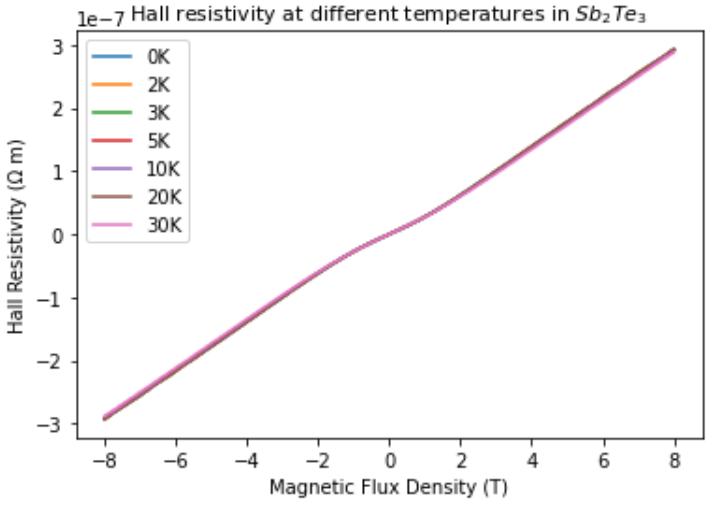

Figure 3.3: Hall resistivity data at each temperature, showing the negligible change due to change in temperature

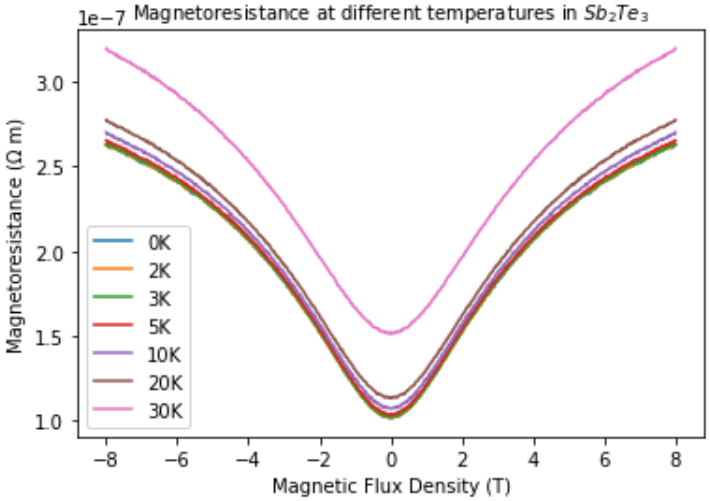

Figure 3.4: Magnetoresistance data at each seven different temperatures from 0K to 30K in a sample of Sb_2Te_3. The data shows the mobility is dependent on temperature

The magnetoresistance data shows a non-linear resistivity dependence on temperature as expected [25][26]. The Hall data is also non-linear, with minimal change in the Hall resistance values with the change in magnetic flux density. Due to the uncertainty of the 2-band model fitting and the extremely small change with temperature, it was not possible to use the 2-band fit to obtain the mobility at each temperature whilst obtaining results to see a coherent trend. Another method was used instead, considering the relationship between mobility and resistivity at zero field.

$$\rho(T, B = 0) \cdot ne = \frac{1}{\mu} \tag{3.1}$$

The resistivity is inversely proportional to carrier density n and mobility μ at zero field. However, one can approximate that the carrier density is a constant value because of the negligible change in the Hall resistivity data. This approximation can be made because the carrier density is related to the Hall Coefficient which is the gradient of the Hall data.

$$R_H = \frac{1}{ne} \tag{3.2}$$

As a result of this approximation, a graph can be plotted of the percentage change in mobility relative to 0K by taking the magnetoresistance values for each temperature at zero field.

3.1.4 Mobility dependence on temperature

Due to the approximation from the previous section, the percentage change in mobility graph can be plotted which shows an exponential decrease in mobility with an increase in temperature. This relationship makes sense as one may assume that this would be due to increasing electron and phonon scattering events. WAL effects would also be expected to have an impact on the temperature dependant magnetoresistance data, since it has been shown that Sb_2Te_3 does show WAL behaviour, yet none can be seen in this data [27]. Regardless, this analysis shows that the efficiency of a high-performance device using Sb_2Te_3 would definitely be effected due to an increase in temperature from 0K.

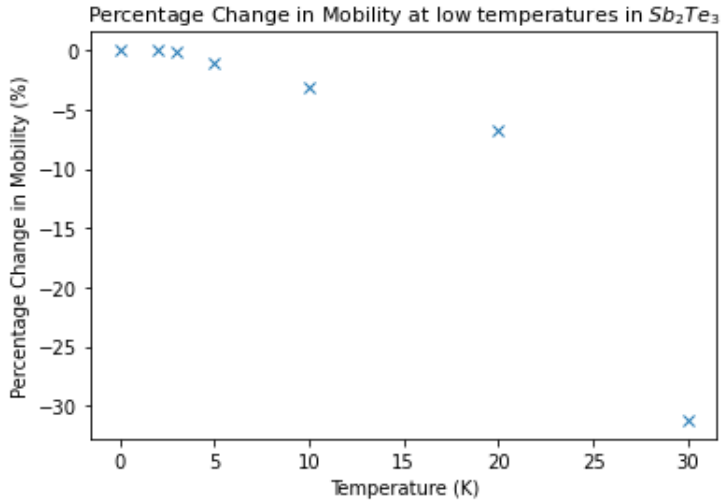

Figure 3.5: Percentage change in mobility of a sample of Sb_2Te_3 at seven different temperatures from 0K to 30K. The graph shows an exponential decrease in the mobility due to increasing temperature

3.2 Bismuth (III) Selenide

3.2.1 Hall data

The second sample examined was Bi_2Se_3, where the primary aim was to extract the mobility and carrier density of the sample. Bi_2Se_3 is a simple TI with regard to its band structure, only requiring the one band model due to its linear Hall data.

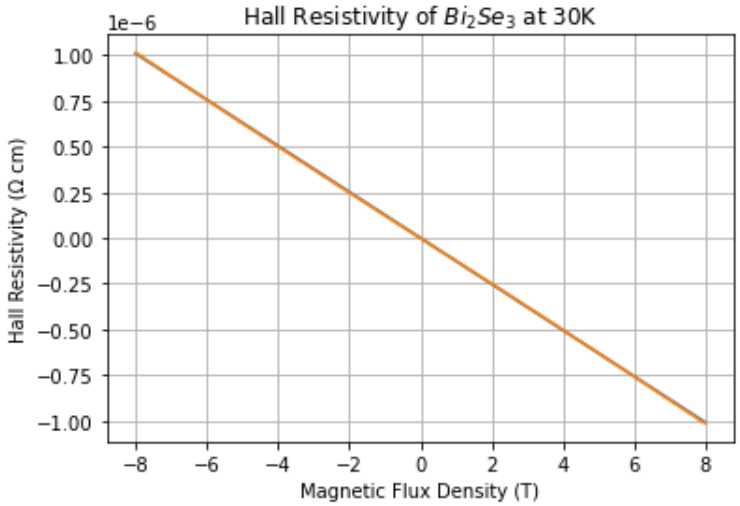

Figure 3.6: Hall data of Bi_2Se_3, illustrating the negative linear gradient

The carrier density can also be calculated from the Hall coefficient of $(-1.26 \pm 0.01) \times 10^{-7} m^3 C^{-1}$ which is the gradient of the Hall resistivity graph. The negative Hall coefficient also shows that this sample of Bi_2Se_3 is an n-type TI meaning that electrons are the majority charge carrier. Using equation 3.2 the carrier density calculated is $(4.94 \pm 0.01) \times 10^{19} cm^{-3}$.

3.2.2 Magnetoresistance data

The results from the one-band model show a mobility of $(274 \pm 5) cm^2 V^{-1} s^{-1}$. The noise from the sample also creates quite a large uncertainty in the fitting. The mobility value obtained is relatively low compared to what would be expected from Bi_2Se_3 [28][14] or a semiconductor such as Silicon which has a mobility of the order of $1000 cm^2 V^{-1} s^{-1}$[29]. This would suggest that mobility of the sample of Bi_2Se_3 is mostly influenced by the bulk of the material, as the mobility of the surface state would be a lot higher.

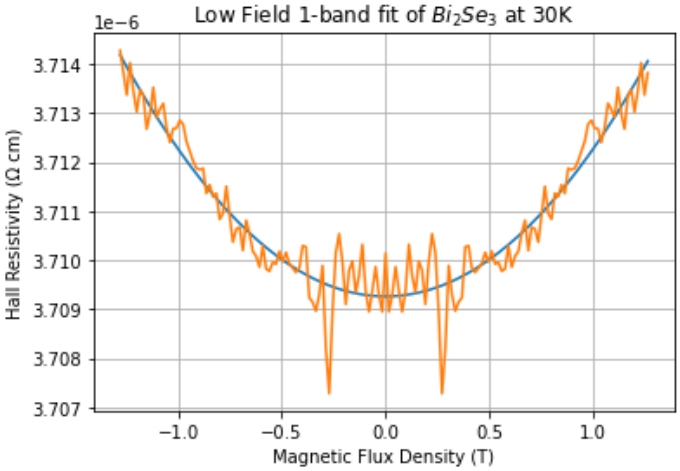

Figure 3.7: Magnetoresistance data of Bi_2Se_3 shown at low field, requiring the 1-band model

3.2.3 Linear magnetoresistance

The magnetoresistance data shown by the Bi_2Se_3 sample shows a very important characteristic of TI's, especially for high-performance devices, which is that it is linear. The linear magnetoresistance implies that Bi_2Se_3 at low temperature shows a linear dispersion relation between the energy and wavevectors of fermions, which aligns with the Dirac model [30]. This provides evidence this TI has a dispersion relation where the values close to the Fermi level can be modelled as a Dirac cone. However, to definitively state whether the origin of the linear magnetoresistance is from Dirac fermions, angular dependant magnetoresistance measurements must be taken [28][30].

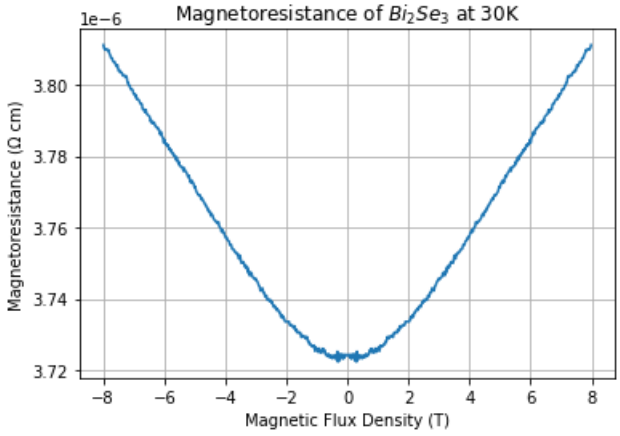

Figure 3.8: Linear magnetoresistance of Bi_2Se_3

3.2.4 Shubnikov–de Haas oscillations

Using the same sample of Bismuth (III) Selenide at 0K, SdH oscillations can be observed at high magnetic fields. This proves the existence of quantum spin Hall states as the oscillations indicate the quantisation of the density of states into Landau levels, where further analysis will increasingly reinforce this.

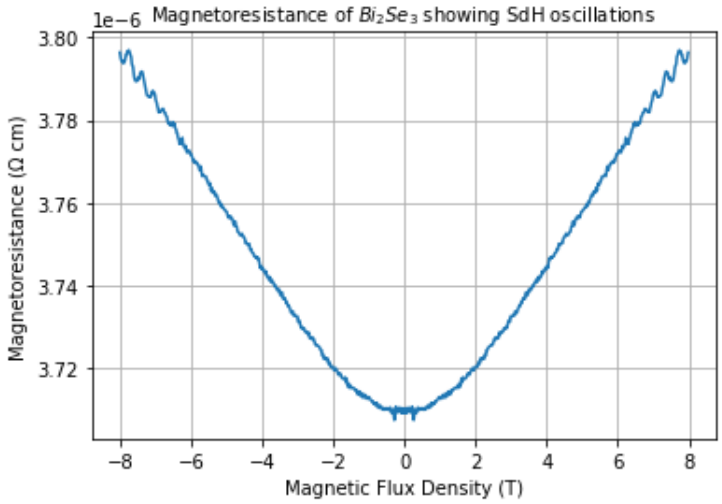

Figure 3.9: Magnetoresistance of Bi_2Se_3 at 0K, showing SdH oscillations beginning at approximately ± 6T

The next stage of analysis requires a Fourier transform to be carried out on the magnetoresistance data so that the quantum oscillation frequency can be obtained. The frequency from the Fourier analysis is 154.2 T.

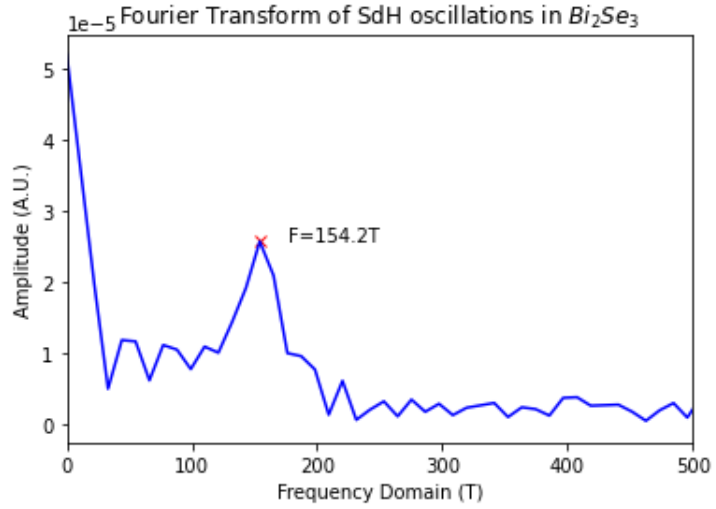

Figure 3.10: Fourier analysis of the Bi_2Se_3 magnetoresistance data, showing the oscillation frequency at 154.2T

A Landau fan diagram can be plotted to show the oscillations in a discrete manner, using the oscillation frequency found using the Fourier Transform. To find the Landau level index N at 8T, the conductivity data was fitted to the Cosine function, making use of the Lifshitz Kosevich theory.

The Landau Fan diagram attempts to demonstrate the non-trivial topological surface state in this sample of Bi_2Se_3 from the value of the Berry phase. Unfortunately, since the Landau index numbers in the fan diagram are large, the value for the Berry phase extracted cannot be used to definitively show non-trivial topology, as it is too inaccurate.

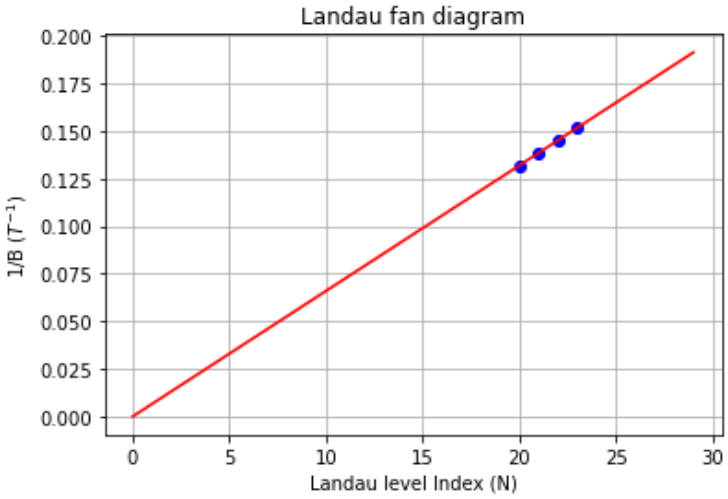

Figure 3.11: Landau fan diagram showing the quantum oscillations in Bi_2Se_3 at low temperature with the points indicating the minima of the oscillations. The line intersects the x-axis at the value of 0.009 which is the Berry phase.

Evidence to attempt to show that there are Dirac fermions in surface state of this sample can be obtained through a linear fitting of the Landau fan diagram, to show where the line intersects with the x-axis. The value of the x intersect which is found to be 0.009 corresponds to the Berry phase, which should take a value of 0.5 or π that is expected from Dirac fermions [10][31]. The value from the fitting is relatively far off the value expected, as it has been proven previously that Bi_2Se_3 does contain a Dirac surface state [32][33]. Despite the inaccuracy due the oscillations being at large Landau index numbers, the value for the Berry phase is an accurate value to support a non-Dirac surface state which should take a value of 0.

From the quantum oscillation frequency acquired from the Fourier Transform, one can also calculate the Fermi wavevector k_F through Onsager's relation [19] which is given as

$$F = \frac{k_F^2}{2e} \tag{3.3}$$

From this relation the Fermi wavevector takes a value of $7.0 \times 10^6 m^{-1}$. This should enable the calculation of the carrier density of the surface state n_s, however from the value of the Berry phase and low mobility from the 1-band fit, one can deduce that the quantum oscillations observed were due to the bulk 3D Fermi surface. A method to confirm this would be through analysis of angular dependant magnetoresistance oscillations [28], although this data was not available. The carrier density of the bulk 3D Fermi surface n is calculated using the following equation:

$$k_F = (3\pi^2 n)^{\frac{1}{3}} \tag{3.4}$$

The carrier density obtained through this equation is $1.2 \times 10^{19} cm^{-3}$. Accounting for spin degeneracy in the non-topological 3D Fermi surface [10], the final carrier density obtained $2.4 \times 10^{19} cm^{-3}$. This compares to the carrier density obtained in section 4.1 from the Hall data which was $5.0 \times 10^{19} cm^{-3}$. This is a high value which supports which the fact that there is no 2D Dirac surface state observed, as the high bulk carrier density results in a lower bulk resistivity, meaning for this sample only the bulk can be observed.

Chapter 4

Conclusions

4.1 Bismuth (III) Selenide

The Bi_2Se_3 sample was unfortunately unable to produce topological behaviour as was expected and has been proved in other studies [14][10][31]. The mobility of the sample was calculated to be only $(274 \pm 5) cm^2 V^{-1} s^{-1}$ which is low for what should be expected from the surface state [28][14], as well as the carrier density being $(4.94 \pm 0.01) \times 10^{19} cm^{-3}$ which is higher than from other research [28][34]. The SdH analysis of this sample also aligned with the mobility value obtained from the 1-band fit, due to the Berry phase not being that expected of Dirac fermions. From this analysis one can conclude that although a high mobility Dirac surface state has been proved in Bi_2Se_3, in this sample the conductivity from the bulk far outweighed that of the surface state, which resulted in the surface state contribution not being noticeable. This is most likely due to the high carrier density of the bulk state. From this it can also be concluded that the SdH oscillations observed were from a bulk 3D Fermi surface, instead of from the 2D surface state. It is likely that the reason a Dirac surface state was not observed is due to the modified Bridgman method which was used to synthesise the sample. Molecular beam epitaxy (MBE) grown films are usually favoured to observe high mobility surface states because it is of higher quality with lack of defects, as well as having a high surface to bulk ratio [35][30]. Despite this, linear magnetoresistance was observed at low temperatures which is an important quality of TI's and does provide some evidence for a linear dispersion relation which indicates the possibility of a Dirac cone [30][36].

4.2 Antimony (III) Telluride

Sb_2Te_3 with a very high carrier density of $(1.74 \pm 0.01) \times 10^{20} cm^{-3}$ showed a clear relationship between the change in mobility with temperature from the magnetoresistance data. Interestingly the Hall data showed negligible temperature dependence which allowed for the assumption of a constant surface and bulk carrier density, enabling a plot of percentage change in mobility to be created. The plot showed an exponential decrease in mobility with temperature which agrees with other research [26][25] showing resistivity dependence on temperature. This relationship would be expected as there more factors contributing to electrical resistivity as temperatures increase, such as phonon-phonon and electron-phonon scattering events in the surface state. Depending on the bulk contribution to resistivity there may also be electron-electron scattering events, as these events are dramatically reduced in the surface state due to topological protection. Unfortunately, it cannot be assumed that the surface state does have a meaningful contribution to the overall conductivity even with a high obtained mobility value, due to the lack of SdH oscillations in the magnetoresistance data.

4.3 High-performance electronics

This study has proven that the future use of TI's in high-performance devices will not come without challenges. The Bi_2Se_3 sample showed that it must be of very high quality to gain the high mobility desired by future devices through the Dirac surface state [30]. It will undoubtedly require further developments to drive down manufacturing costs of high-quality TI's. The sample of Sb_2Te_3 showed a decrease in mobility with an increase in temperature. Although the temperatures in this report were not close to room temperature, it is clear to see that device performance due to charge mobility decreases with an increase in temperature may be something to consider when creating room temperature TI devices.

4.4 Future research

A key setback for creating high-performance devices from TI's that has been realised through this report, is need for high quality TI's which will enable the device to make use of the high mobility surface state. Future work is required for lowering the bulk carrier density to enable more conduction through the surface state, as well as creating cheaper methods for fabricating high quality samples. MBE is an excellent method for achieving high quality samples, hence developments must be made to reduce the cost and make it more available. More research must also be done to enhance the potential of the surface state for optimal transistor performance, for example by increasing the number of electrons in the surface state [37].

Bibliography

[1] Bastian Höckendorf, Andreas Alvermann, and Holger Fehske. Topological invariants for floquet-bloch systems with chiral, time-reversal, or particle-hole symmetry. *Physical Review B*, 97(4):045140, 2018.

[2] A. Al Bayaz, A. Giani, A. Foucaran, F. Pascal-Delannoy, and A. Boyer. Electrical and thermoelectrical properties of bi2se3 grown by metal organic chemical vapour deposition technique. *Thin Solid Films*, 441(1):1–5, 2003.

[3] Zhijie Zhang, Wenzhong Wang, Lu Wang, and Songmei Sun. Enhancement of visible-light photocatalysis by coupling with narrow-band-gap semiconductor: a case study on bi2s3/bi2wo6. *ACS applied materials & interfaces*, 4(2):593–597, 2012.

[4] Liangzhi Kou, Binghai Yan, Feiming Hu, Shu-Chun Wu, Tim O Wehling, Claudia Felser, Changfeng Chen, and Thomas Frauenheim. Graphene-based topological insulator with an intrinsic bulk band gap above room temperature. *Nano letters*, 13(12):6251–6255, 2013.

[5] Stephan Rachel and Karyn Le Hur. Topological insulators and mott physics from the hubbard interaction. *Phys. Rev. B*, 82:075106, Aug 2010.

[6] Charles L Kane and Eugene J Mele. Physics. a new spin on the insulating state. *Science (New York, NY)*, 314(5806):1692–3, 2006.

[7] Zhihua Yang and Jung Hoon Han. Landau level states on a topological insulator thin film. *Physical Review B*, 83(4):045415, 2011.

[8] Shigeji Fujita and Akira Suzuki. Theory of shubnikov-de haas and quantum hall oscillations in graphene under bias and gate voltages. *Global Journal of Science Frontier Research*, 14, 2014.

[9] Yong P Chen. Topological insulator-based energy efficient devices. In *Micro-and Nanotechnology Sensors, Systems, and Applications IV*, volume 8373, page 83730B. International Society for Optics and Photonics, 2012.

[10] Yoichi Ando. Topological insulator materials. *Journal of the Physical Society of Japan*, 82(10):102001, 2013.

[11] Luis Brey and HA Fertig. Electronic states of graphene nanoribbons studied with the dirac equation. *Physical Review B*, 73(23):235411, 2006.

[12] Hendrik Antoon Kramers. Théorie générale de la rotation paramagnétique dans les cristaux. *Proc. Acad. Amst*, 33(6), 1930.

[13] H Mirhosseini, M Flieger, and J Henk. Dirac-cone-like surface state in w (110): dispersion, spin texture and photoemission from first principles. *New Journal of Physics*, 15(3):033019, 2013.

[14] Dong-Xia Qu, Yew San Hor, Jun Xiong, Robert Joseph Cava, and Nai Phuan Ong. Quantum oscillations and hall anomaly of surface states in the topological insulator bi2te3. *Science*, 329(5993):821–824, 2010.

[15] Xi Chen, Ke He, Xucun Ma, and Qikun Xue. Scanning tunneling microscopy studies of topological insulators grown by molecular beam epitaxy. In *EPJ Web of Conferences*, volume 23, page 00020. EDP Sciences, 2012.

[16] Paul Adrien Maurice Dirac. *The principles of quantum mechanics*. Number 27. Oxford university press, 1981.

[17] Shinobu Hikami, Anatoly I Larkin, and Yosuke Nagaoka. Spin-orbit interaction and magnetoresistance in the two dimensional random system. *Progress of Theoretical Physics*, 63(2):707–710, 1980.

[18] J Angevaare. The weak anti localization effect due to topological surface states of a bi1.46sb0.54te1.7se1.3 nanoflake, 2014.

[19] David Shoenberg. *Magnetic oscillations in metals*. Cambridge university press, 2009.

[20] Jiamin Xue. Berry phase and the unconventional quantum hall effect in graphene, 2013.

[21] Joshua Gretton. personal communication.

[22] Neil W Ashcroft, N David Mermin, et al. *Solid state physics*, volume 2005. holt, rinehart and winston, new york London, 1976.

[23] Nicola Peranio, Markus Winkler, Dimitrios Bessas, Zainul Aabdin, J König, Harald Böttner, RP Hermann, and Oliver Eibl. Room-temperature mbe deposition, thermoelectric properties, and advanced structural characterization of binary bi2te3 and sb2te3 thin films. *Journal of alloys and compounds*, 521:163–173, 2012.

[24] A Giani, A Boulouz, F Pascal-Delannoy, A Foucaran, E Charles, and A Boyer. Growth of bi2te3 and sb2te3 thin films by mocvd. *Materials Science and Engineering: B*, 64(1):19–24, 1999.

[25] P. Dutta, D. Bhoi, A. Midya, N. Khan, P. Mandal, S. Samatham, and V. Ganesan. Anomalous thermal expansion of sb2te3 topological insulator. *Applied Physics Letters*, 100:251912, 2012.

[26] Yi-Chi Huang, PC Lee, CH Chien, FY Chiu, YY Chen, and Sergey R Harutyunyan. Magnetotransport properties of sb2te3 nanoflake. *Physica B: Condensed Matter*, 452:108–112, 2014.

[27] Rabia Sultana, Ganesh Gurjar, S Patnaik, and VPS Awana. Crystal growth and characterization of bulk sb2te3 topological insulator. *Materials Research Express*, 5(4):046107, 2018.

[28] Kazuma Eto, Zhi Ren, AA Taskin, Kouji Segawa, and Yoichi Ando. Angular-dependent oscillations of the magnetoresistance in bi 2 se 3 due to the three-dimensional bulk fermi surface. *Physical Review B*, 81(19):195309, 2010.

[29] GW Ludwig and RL Watters. Drift and conductivity mobility in silicon. *Physical Review*, 101(6):1699, 1956.

[30] Y Shiomi and E Saitoh. Linear magnetoresistance in a topological insulator ru2sn3. *AIP Advances*, 7(3):035011, 2017.

[31] AA Taskin, Satoshi Sasaki, Kouji Segawa, and Yoichi Ando. Manifestation of topological protection in transport properties of epitaxial bi 2 se 3 thin films. *Physical review letters*, 109(6):066803, 2012.

[32] Yuan Yan, Zhi-Min Liao, Yang-Bo Zhou, Han-Chun Wu, Ya-Qing Bie, Jing-Jing Chen, Jie Meng, Xiao-Song Wu, and Da-Peng Yu. Synthesis and quantum transport properties of bi 2 se 3 topological insulator nanostructures. *Scientific reports*, 3(1):1–5, 2013.

[33] David Hsieh, Yuqi Xia, Dong Qian, L Wray, JH Dil, Fedorov Meier, J Osterwalder, L Patthey, JG Checkelsky, Nai Phuan Ong, et al. A tunable topological insulator in the spin helical dirac transport regime. *Nature*, 460(7259):1101–1105, 2009.

[34] Sungjae Cho, Nicholas P Butch, Johnpierre Paglione, and Michael S Fuhrer. Insulating behavior in ultrathin bismuth selenide field effect transistors. *Nano letters*, 11(5):1925–1927, 2011.

[35] Theresa P Ginley, Yong Wang, and Stephanie Law. Topological insulator film growth by molecular beam epitaxy: A review. *Crystals*, 6(11):154, 2016.

[36] David Hsieh, Yuqi Xia, D Qian, L Wray, Fabian Meier, JH Dil, J Osterwalder, L Patthey, AV Fedorov, H Lin, et al. Observation of time-reversal-protected single-dirac-cone topological-insulator states in bi 2 te 3 and sb 2 te 3. *Physical review letters*, 103(14):146401, 2009.

[37] L Andrew Wray. Topological transistor. *Nature Physics*, 8(10):705–706, 2012.